ACS APPLIED MATERIALS & INTERFACES

Research Article

www.acsami.org

Enhanced Performance of Layered Titanate Nanowire-Based Supercapacitor Electrodes by Nickel Ion Exchange

Weijia Zhou,*[,†] Xiaojun Liu,[†] Yuanhua Sang,[‡] Zhenhuan Zhao,[‡] Kai Zhou,[†] Hong Liu,[‡] and Shaowei Chen*[,†,§]

[†]New Energy Research Institute, School of Environment and Energy, South China University of Technology, Guangzhou Higher Education Mega Center, Guangzhou, Guangdong 510006, China

[‡]State Key Laboratory of Crystal Materials, Center of Bio & Micro/Nano Functional Materials, Shandong University, 27 Shandanan Road, Jinan, Shandong 250100, China

[§]Department of Chemistry and Biochemistry, University of California, 1156 High Street, Santa Cruz, California 95064, United States

Supporting Information

ABSTRACT: Titania nanostructured materials have been used extensively for the fabrication of electrochemical capacitors. However, the devices typically exhibit relatively low capacitance and poor cycling stability. Herein, we report the synthesis of a core−shell heterostructure based on layered titanate nanowires coated with nickel hydroxide nanosheets on a titanium mesh, referred to as $K_2Ti_4O_9$@$Ni(OH)_2$/Ti, by a simple nickel ion exchange reaction. The incorporation of nickel into the titanate nanowires is confirmed by X-ray photoelectron spectroscopic measurements and elemental mapping. Scanning electron microscopic and transmission electron microscopic measurements show the formation of a highly porous network of the hybrid nanowires. Electrochemical studies show that the $K_2Ti_4O_9$@$Ni(OH)_2$/Ti electrodes possess a high specific capacitance of 340 mF/cm^2 at 50 mV/s in an aqueous electrolyte of 3 M KOH and 3 mF/cm^2 at 0.04 mA/cm^2 in the KOH/PVA solid-state electrolyte, with an excellent retention rate of 92.5% after 2000 cycles and 92.7% after 10 000 cycles, respectively. Such a performance is a few tens of times better than that of the unmodified $K_2Ti_4O_9$/Ti electrode. The enhanced capability of the chemically modified titanate electrodes may open up new opportunities in the development of low-cost, high-performance, and flexible supercapacitors.

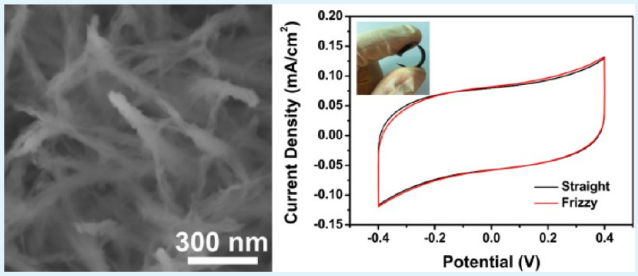

KEYWORDS: *titanate nanowire, ion exchange, $Ni(OH)_2$ nanosheet, supercapacitor*

INTRODUCTION

Energy storage and conversion from alternative energy sources has been attracting extensive interest in both fundamental research and technological development. Among these, supercapacitors represent one of the most ideal candidates for green energy storage because of their high power density, superhigh cycling life, and safety of operation.[1−3] On the basis of the charge storage mechanism, supercapacitors are generally divided into two categories, electrical double-layer capacitors (EDLCs) mostly based on carbon-active materials of high electrical conductivity and large surface areas[4,5] and pseudocapacitors based on redox-active materials (e.g., MnO_2, Co_3O_4, and $Ni(OH)_2$).[6−8]

Among these, tremendous efforts have been devoted to the development of one-dimensional inorganic nanomaterials as supercapacitor electrodes, such as TiO_2,[9] Co_3O_4,[10] MnO_2,[11] Ni_3S_2,[12] and RuO_2,[13] largely because of their large surface area as well as effective pathways for charge transport. For instance, titanate (e.g., $K_2Ti_4O_9$, $K_2Ti_3O_7$, and $H_2Ti_3O_7$) has been widely used in ion intercalation,[14] photocatalysis,[15,16] and lithium ion batteries,[17] and titanate nanowires with a layered structure have been proposed as a promising alternative for supercapacitor applications due to the open layered structure and short diffusion paths for ions and electrons.[18] In the layered structure of titanate, cations (K^+, Na^+, and H^+) occupy the cavities between the layers of the TiO_6 octahedra, leading to high conductivity along the interlayer direction. Meanwhile, exchange reactions can be carried out with transition-metal ions (e.g., Co^{2+}, Ni^{2+}, and Cu^{2+}), resulting in ion entrapment between the open layers of titanate.[14] Interestingly, such ion intercalation does not impact the interlayer distance, indicating that the rigidity of the titanate framework can be maintained during the ion exchange and charging/discharging cycles.

To further enhance the surface area and surface accessibility to electrolyte ions, the nanowires are generally engineered into three-dimensional (3D) nanostructures, which provide more efficient contacts between the electrolyte ions and the active materials. In fact, various 3D hybrid nanostructures, such as

Received: January 20, 2014
Accepted: March 4, 2014
Published: March 4, 2014

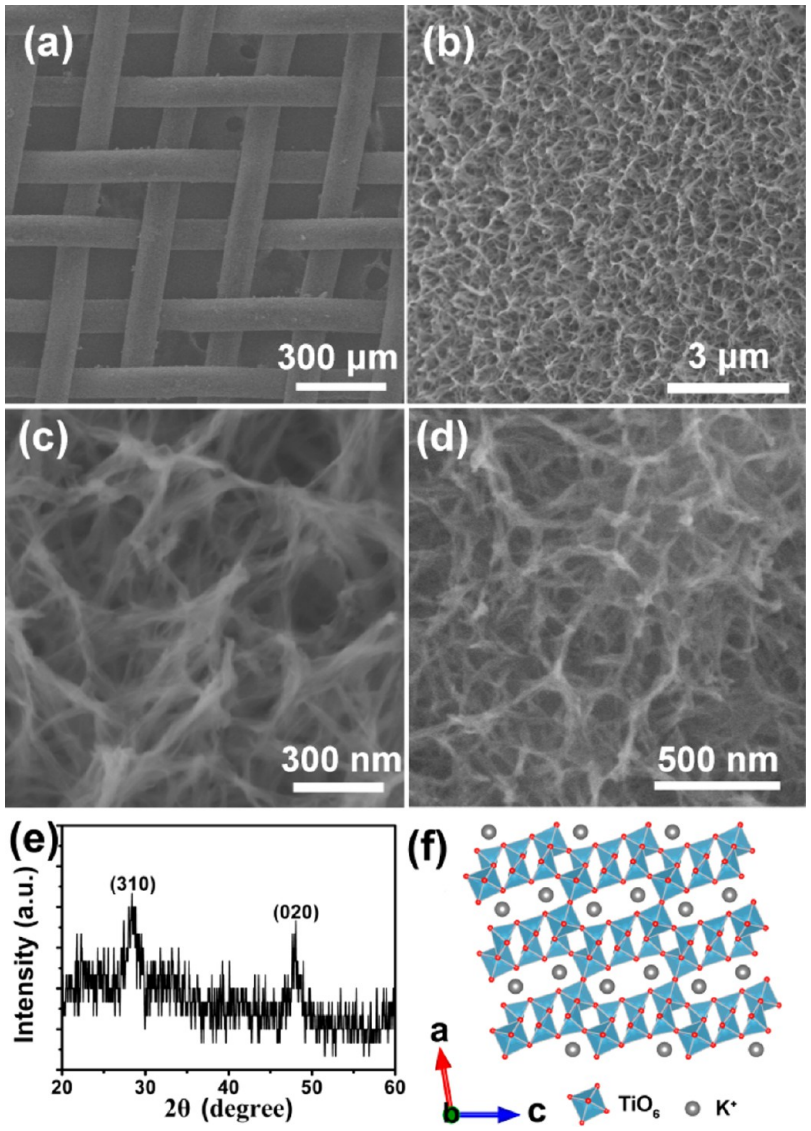

Figure 1. SEM micrographs of (a–c) $K_2Ti_4O_9$/Ti and (d) TiO_2/Ti. (e) XRD patterns of $K_2Ti_4O_9$ powders scratched from $K_2Ti_4O_9$/Ti mesh, and (f) schematic structure of $K_2Ti_4O_9$.

Co_3O_4@MnO_2,[10] Ni_3S_2@$Ni(OH)_2$,[12] and CoO@NiHON,[19] have been reported to significantly enhance both the capacitance and durability of supercapacitors. In the present work, layered titanate $K_2Ti_4O_9$ nanowires were synthesized by way of a low temperature reaction, and a 3D hybrid structure of titanate nanowires coated with nickel hydroxide nanosheets ($K_2Ti_4O_9$@$Ni(OH)_2$/Ti) was obtained by way of a simple nickel ion-exchange reaction, which was confirmed by X-ray photoelectron spectroscopic (XPS) measurements and elemental mapping. Scanning electron microscopic (SEM) and transmission electron microscopic (TEM) measurements showed the formation of a highly porous network of the hybrid nanowires. With effective ion intercalation, the materials were found to serve as a promising candidate as sodium ion battery and supercapacitor electrodes.[20,21] Electrochemical studies in an aqueous solution of 3 M KOH showed that $K_2Ti_4O_9$/Ti exhibited an areal capacitance of 5 mF/cm^2 at a potential scan rate of 50 mV/s. After Ni^{2+} intercalation, the areal capacitance of the $K_2Ti_4O_9$@$Ni(OH)_2$/Ti composite electrodes was found to increase dramatically by about 70 times to 340 mF/cm^2. Such a performance was markedly higher than those of earlier studies of TiO_2-based electrochemical capacitors,[7,9,22−24] where the specific capacitances are typically very low, as a result of their poor electrochemical activity and low electrical conductivity.[25] The results suggest that interfacial engineering of electrode materials may be an effective route to the manipulation and enhancement of supercapacitor performance.

EXPERIMENTAL SECTION

Materials. All reagents were of analytical grade and used without further purification. Potassium hydroxide (KOH), hydrochloric acid (HCl), nickel nitrate ($Ni(NO_3)_2$), and poly(vinyl alcohol) (PVA, molecular weight 75 000−80 000) were obtained from Sinopharm Chemical Reagents Co., Ltd. in China. Ti meshes (99.9% purity) were obtained from Shengzhuo Titanium Mesh Products Co., Ltd. in China. Water was supplied with a Barnstead Nanopure Water System (18.3 MΩ cm).

Preparation of $K_2Ti_4O_9$/Ti and $K_2Ti_4O_9$@$Ni(OH)_2$/Ti. Ti meshes (3 × 1 cm^2) were cleaned by sonication in acetone and ethanol, respectively, rinsed with deionized water, and finally dried at 60 °C. The dried Ti mesh was then put into a sealed glass bottle loaded with 20 mL of a 10 M KOH solution in an electric oven at 90 °C for 6 h

dx.doi.org/10.1021/am500421r | ACS Appl. Mater. Interfaces 2014, 6, 4578−4586

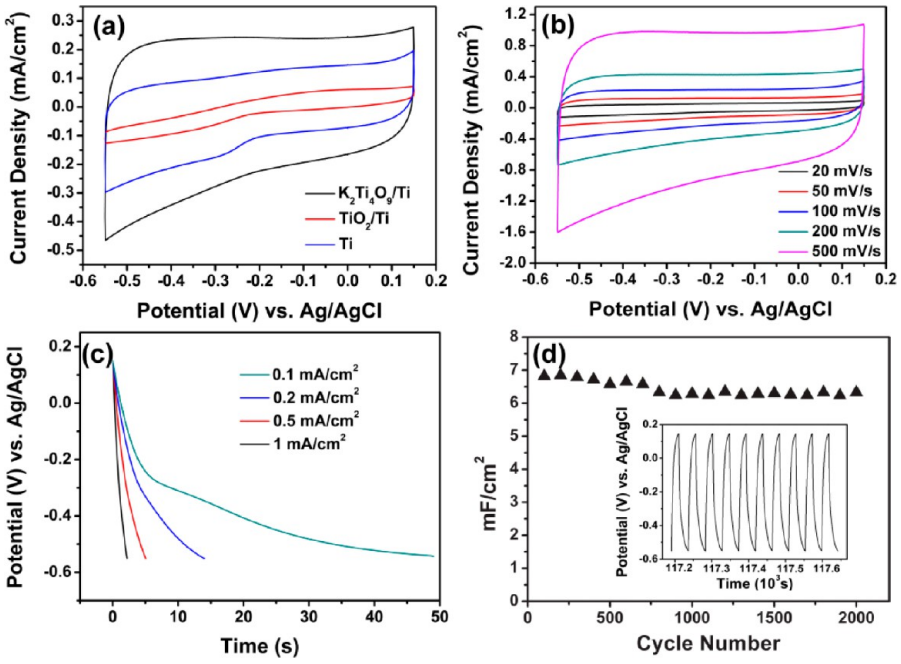

Figure 2. (a) CV curves of the $K_2Ti_4O_9$/Ti, TiO_2/Ti, and Ti obtained at a scan rate of 100 mV/s in an aqueous solution of 3 M KOH. (b) CV curves of $K_2Ti_4O_9$/Ti at various potential scan rates. (c) Galvanostatic discharge curves of a $K_2Ti_4O_9$/Ti sample collected as a function of current density. (d) Cycling stability of a $K_2Ti_4O_9$/Ti sample at a current density of 0.1 mA/cm^2. Inset: The last 10 charge−discharge curves of $K_2Ti_4O_9$/Ti.

under autogenous pressure and static conditions and air-cooled to room temperature. The samples were washed with deionized water several times to obtain $K_2Ti_4O_9$/Ti, which was then immersed into a 1 M $Ni(NO_3)_2$ solution at 80 °C for 12 h and rinsed repeatedly with Nanopure water several times to produce ion intercalated $Ni_xK_{2-x}Ti_4O_9$/Ti (x is the number of ion replacement). $K_2Ti_4O_9$@$Ni(OH)_2$/Ti was finally obtained by an electrochemical activation process by potential sweeping for 2000 cycles at a scan rate of 100 mV/s in a 3 M KOH aqueous solution.

As a reference sample, TiO_2/Ti was prepared by acid washing of the obtained $K_2Ti_4O_9$/Ti, then thermal annealing at 450 °C for 2 h.

Characterizations. Surface morphologies of the samples were studied with a Hitachi S-4800 field emission scanning electron microscope (FESEM). The chemical composition was investigated by energy-dispersive X-ray spectroscopic (EDX) and X-ray photoelectron spectroscopic (XPS, ESCALAB 250) measurements. Powder X-ray diffraction (XRD) patterns of the $K_2Ti_4O_9$ powders exfoliated from $K_2Ti_4O_9$/Ti were recorded on a Bruker D8 Advance powder X-ray diffractometer with Cu Ka radiation (λ = 0.15406 nm). High-resolution transmission electron microscopic (HRTEM) images were acquired using a JEOL JEM-2100 instrument working at an acceleration voltage of 200 kV.

Electrochemistry. Cyclic voltammetry (CV), galvanostatic charging/discharging, and electrochemical impedance spectroscopy (EIS) tests were performed in a 3 M KOH aqueous solution with a CH Instruments electrochemical workstation (Model CHI 660E). The working electrode was the above-obtained $K_2Ti_4O_9$/Ti or $K_2Ti_4O_9$@$Ni(OH)_2$/Ti (0.5 cm^2), and a Ag/AgCl (in saturated KCl) and a Pt wire were used as the reference and counterelectrodes, respectively.

Areal capacitances are calculated from the CV and charge−discharge curves by way of eqs 1 and 2, respectively, where I_1 is the response current, ΔV is the voltage window, ν is the scan rate, I_2 is the constant discharge current, Δt is the discharging time, and S is the geometrical area of the Ti mesh electrode (1 × 0.5 cm^2):

$$C_{S1} = \frac{\int I_1 \, dV}{\nu S \Delta V} \quad (1)$$

$$C_{S2} = \frac{I_2 \Delta t}{S \Delta V} \quad (2)$$

The specific capacitance of $K_2Ti_4O_9$/Ti and $K_2Ti_4O_9$@$Ni(OH)_2$/Ti was estimated by normalizing the capcitance to the mass (m) of the active materials that was about 0.12 mg ($K_2Ti_4O_9$) and 0.42 mg ($K_2Ti_4O_9$@$Ni(OH)_2$), respectively. The equations are simlar with eqs 1 and 2, but instead of S, m is substituted. The energy density (E) and Power density (P) are calculated by eqs 3 and 4, respectively:

$$E = \frac{1}{2} C_m (\Delta V)^2 \quad (3)$$

$$P = E/\Delta t \quad (4)$$

Solid-State Supercapacitors. To prepare solid-state supercapacitors, an alkaline KOH/PVA polymer electrolyte were used which entailed 3 g of PVA and 2 g of KOH dissolved in 30 mL of Nanopure water under vigorous continuous stirring at 85 °C. Two pieces of $K_2Ti_4O_9$@$Ni(OH)_2$/Ti (0.5 × 1 cm^2) were partially (0.5 × 0.5 cm^2) immersed into the KOH/PVA solution for 5 min, taken out, and then assembled face-to-face. When the electrolyte became solidified at room temperature, a solid-state symmetrical supercapacitor was obtained.

RESULTS AND DISCUSSION

As mentioned above, $K_2Ti_4O_9$ nanowires were prepared by simply heating a titanium mesh in an aqueous solution of 10 M KOH at 90 °C for 6 h, which might be converted into TiO_2 by a calcination treatment at 450 °C for 2 h. Figure 1 shows the SEM images of the obtained (a−c) $K_2Ti_4O_9$/Ti and (d) TiO_2/Ti nanostructures. It can be seen that the surface of the Ti mesh (panel a) was covered by a porous network of $K_2Ti_4O_9$ nanowires with diameters in the range of 20 to 50 nm and length of ~1 μm (panels b and c). XRD measurements of the as-grown $K_2Ti_4O_9$ scratched from the Ti mesh (panel e) showed two peaks at 2θ = 28° and 48°, corresponding to the (310) and (020) planes of $K_2Ti_4O_9$, respectively (JCPDS no. 32-0861). Note that $K_2Ti_4O_9$ exhibits a layered structure, where cations (K^+) occupy the cavities between the layers of the TiO_6 octahedra, as shown in the schematic of panel f. Interestingly, when $K_2Ti_4O_9$ was transformed into TiO_2 by thermal annealing

dx.doi.org/10.1021/am500421r | ACS Appl. Mater. Interfaces 2014, 6, 4578−4586

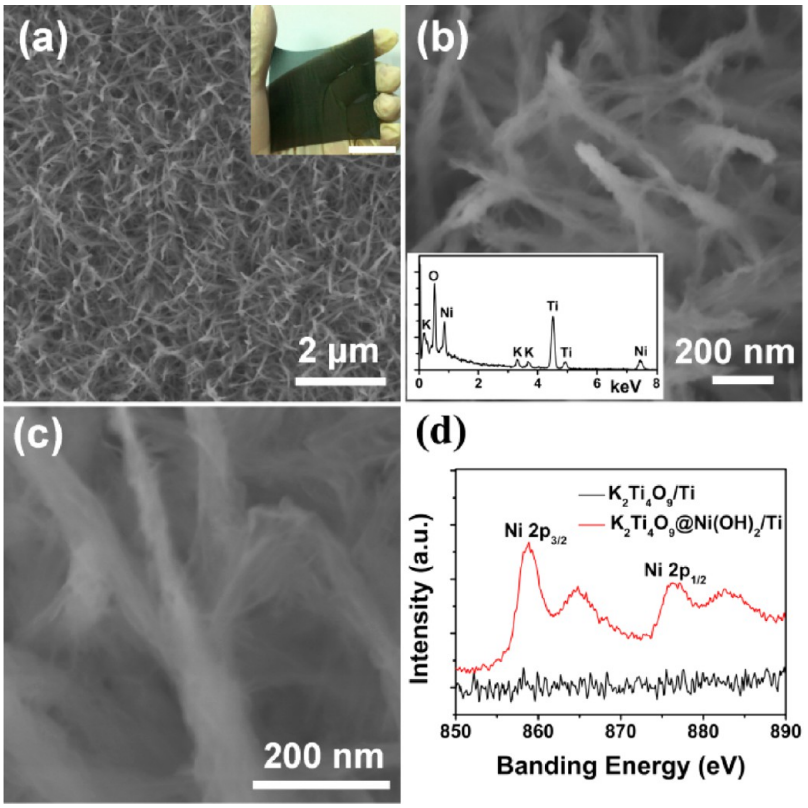

Figure 3. (a) SEM image of $K_2Ti_4O_9$@Ni(OH)$_2$/Ti. Inset is a photograph of a large piece of the $K_2Ti_4O_9$@Ni(OH)$_2$/Ti mesh with a scale bar of 2 cm. (b, c) Magnified SEM images of $K_2Ti_4O_9$@Ni(OH)$_2$. Inset to panel b is the EDS spectrum of $K_2Ti_4O_9$@Ni(OH)$_2$. (d) XPS spectra of $K_2Ti_4O_9$/Ti and $K_2Ti_4O_9$@Ni(OH)$_2$/Ti.

at 450 °C for 2 h, the nanowire morphology did not show apparent differences (panel d), suggesting good thermostability of the nanostructures.

Electrochemical measurements were then carried out to assess the capacitive properties of the $K_2Ti_4O_9$/Ti nanostructures. Figure 2a shows the cyclic voltammograms (CV) of $K_2Ti_4O_9$/Ti, TiO_2/Ti, and Ti recorded at a scan rate of 100 mV/s in an aqueous solution of 3 M KOH. One can see that all CV curves were largely featureless (with a quasi-rectangular shape), indicating primary contributions from double-layer capacitance charging, and the areal capacitances were estimated to be 4.74, 0.54, and 2.49 mF/cm^2 for the $K_2Ti_4O_9$/Ti, TiO_2/Ti, and Ti electrodes, respectively. One can see that the areal capacitance of $K_2Ti_4O_9$/Ti is about 10 times greater than that of TiO_2/Ti, although they exhibit similar morphologies (Figure 1c and d). This is likely because the layered structure of $K_2Ti_4O_9$ (Figure 1f) can effectively accommodate K^+ ions during the charging process. That is, the capacitance of $K_2Ti_4O_9$/Ti likely might entail contributions from both electrical double-layer charging as well as ion exchange of the $K_2Ti_4O_9$/Ti nanowires with electrolyte ions. Figure 2b shows the CV curves of $K_2Ti_4O_9$/Ti at potential scan rates ranging from 20 mV/s to 500 mV/s, which all displayed a quasi-rectangular shape, indicating good rate capability. Yet the areal capacitance was found to decrease somewhat with increasing potential scan rate, e.g., 5.5 mF/cm^2 at 20 mV/s and 3.7 mF/cm^2 at 500 mV/s (Figure S1).

Figure 2c shows the galvanostatic discharge curves of the $K_2Ti_4O_9$/Ti electrode at different current densities. A high specific capacitance (7 mF/cm^2) was obtained at the discharge current density of 0.1 mA/cm^2, and at a relatively high current density of 1 mA/cm^2, a specific capacitance of 3.1 mF/cm^2 can still be obtained. The cycling performance of $K_2Ti_4O_9$/Ti at the current density of 0.1 mA/cm^2 is shown in Figure 2d. At such a current density, the specific capacitance was estimated to be 6.32 mF/cm^2 (corresponding to 93% of the initial value of 6.8 mF/cm^2) after 2000 cycles. The shape of the last 10 charge–discharge curves (inset to Figure 2d) was almost unchanged, indicating excellent cyclability of the $K_2Ti_4O_9$/Ti electrode.

Significantly, the capacitive performance was found to be drastically enhanced by simple ion exchange of the titanate nanowires with Ni^{2+} that formed a core–shell hierarchical nanostructure. As mentioned above, ion-exchange reactions might occur through the open layer structure of $K_2Ti_4O_9$ with transition-metal ions. Experimentally, $K_2Ti_4O_9$@Ni(OH)$_2$/Ti core–shell heterostructures were produced by ion-exchange reactions of $K_2Ti_4O_9$ nanowires with Ni^{2+} in a 1 M $Ni(NO_3)_2$ solution at 80 °C for 12 h, followed by an electrochemical activation process by potential sweeping for 2000 cycles at a scan rate of 100 mV/s in 3 M KOH.

The morphologies and structures of $K_2Ti_4O_9$@Ni(OH)$_2$/Ti were characterized by SEM measurements, as shown in Figure 3a–c. Note that the $K_2Ti_4O_9$@Ni(OH)$_2$/Ti samples could be synthesized on a large scale (inset to Figure 3a). After Ni^{2+} ion-exchange and alkaline reactions, it can be seen that thin Ni(OH)$_2$ nanosheets were formed on the surface of the $K_2Ti_4O_9$ nanowires (Figure 3b and c). Whereas no peaks were observed in XRD measurements for Ni(OH)$_2$ in $K_2Ti_4O_9$@Ni(OH)$_2$/Ti (Figure S2), which was most probably due to small amounts and poor crystallinity, EDS studies clearly revealed the presence of Ti, O, Ni, and K elements in the sample (inset to Figure 3b). XPS measurements further

dx.doi.org/10.1021/am500421r | ACS Appl. Mater. Interfaces 2014, 6, 4578–4586

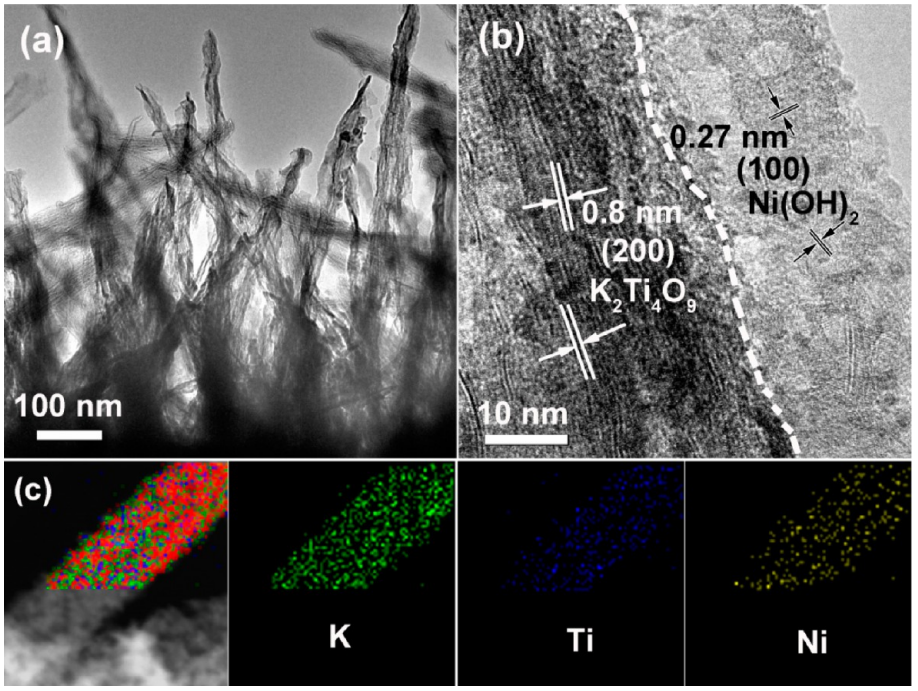

Figure 4. (a) TEM image of $K_2Ti_4O_9$@Ni(OH)$_2$/Ti. (b) HRTEM images of a $K_2Ti_4O_9$ nanowire coated with Ni(OH)$_2$ nanosheets. (c) EDS mapping results from a single heterostructure exfoliated from $K_2Ti_4O_9$@Ni(OH)$_2$/Ti, conforming the core−shell hierarchical structure.

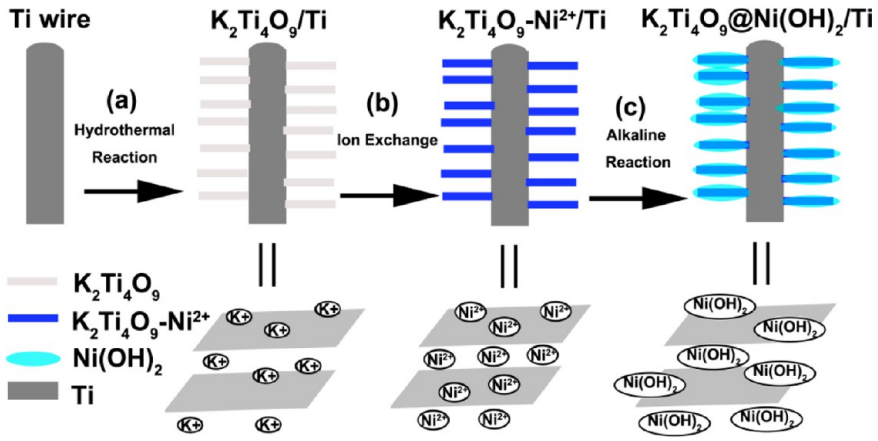

Figure 5. Proposed mechanism for the growth of $K_2Ti_4O_9$@Ni(OH)$_2$/Ti.

confirmed the incorporation of nickel ions in the $K_2Ti_4O_9$ nanowires. From Figure 3d, it can be seen that after nickel ion-exchange reactions, two well-defined peaks emerged at around 859 and 876 eV, which may be assigned to the Ni $2p_{3/2}$ and Ni $2p_{1/2}$ electrons, respectively. The satellite peaks near 865 and 882 eV indicated the presence of Ni^{2+}, most likely in the form of hydrated nickel oxide.[26,27]

The formation of highly porous hierarchical $K_2Ti_4O_9$@ Ni(OH)$_2$ nanostructures was further manifested in TEM measurements. From panel a in Figure 4, it can be seen that the nanowires exhibited a sheet-like morphology of about 50 nm in width and a few hundred nanometers in length. High-resolution imaging in panel b showed well-defined lattice fringes in the interior with a spacing of 0.8 nm that is consistent with the (200) crystal planes of $K_2Ti_4O_9$ (monoclinic, a = 1.83 nm, b = 0.379 nm, c = 1.20 nm) and Ni(OH)$_2$ in the exterior where the lattice fringes of 0.27 nm are in agreement with the Ni(OH)$_2$ (100) planes (hexagonal, $a = b$ = 0.312 nm, c = 0.46 nm). A rather well-defined interface can be identified between the $K_2Ti_4O_9$ nanowires and Ni(OH)$_2$ nanosheets (dashed line in Figure 4b). Note that in the layered structure of $K_2Ti_4O_9$, the (200) crystal faces grew along the axial direction of the nanowires, which is conducive to fast charge transport. The appearance of lattice distortions might be due to Ni^{2+} intercalation. Elemental mapping based on EDS measurements also revealed the formation of a core−shell hierarchical structure of $K_2Ti_4O_9$@Ni(OH)$_2$, as depicted in Figure 4c, where K and Ti can be clearly identified in the backbone region whereas Ni can be found throughout the entire surface.

A possible route to the formation of these hierarchical nanostructures is depicted in Figure 5. During the alkaline hydrothermal process, $K_2Ti_4O_9$ nanowires with an open layered structure were grown on the titanium surface, with K^+ ions distributed on both sides of the TiO_6 octahedra sheets (step a). Ion-exchange reactions with Ni^{2+} then took place between the layers of the nanowires (step b). After the alkaline treatment,

dx.doi.org/10.1021/am500421r | ACS Appl. Mater. Interfaces 2014, 6, 4578−4586

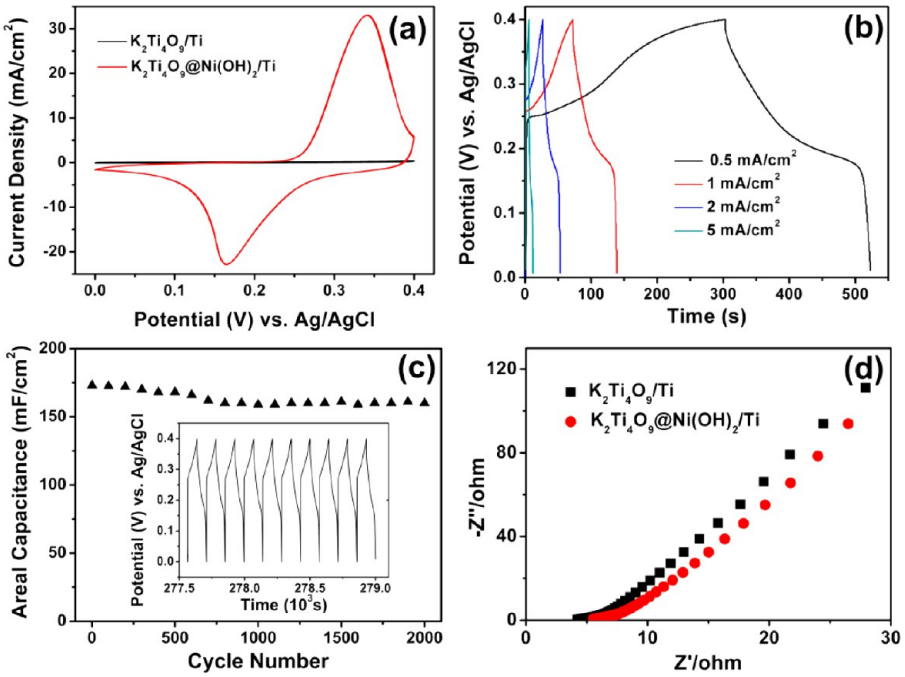

Figure 6. (a) CV curves of $K_2Ti_4O_9$/Ti and $K_2Ti_4O_9$@Ni(OH)$_2$/Ti obtained at a scan rate of 50 mV/s in an aqueous solution of 3 M KOH. (b) Galvanostatic charge/discharge curves of a $K_2Ti_4O_9$@Ni(OH)$_2$/Ti sample collected as a function of current density. (c) Cycling stability of a $K_2Ti_4O_9$@Ni(OH)$_2$/Ti sample at a current density of 1 mA/cm^2. Inset: the last 10 charge/discharge curves of K_2Ti4O_9@Ni(OH)$_2$/Ti. (d) Nyquist plots of the $K_2Ti_4O_9$/Ti and $K_2Ti_4O_9$@Ni(OH)$_2$/Ti electrodes.

Ni(OH)$_2$ nanosheets were produced on the surface of $K_2Ti_4O_9$, leading to the formation of hierarchical $K_2Ti_4O_9$@Ni(OH)$_2$/Ti core–shell nanostructures (step c).

Electrochemical studies showed that the resulting $K_2Ti_4O_9$@Ni(OH)$_2$ heterostructures possessed a markedly higher specific capacitance than the original $K_2Ti_4O_9$. Note that all CV and galvanostatic charge/discharge measurements were carried out after 2000 cycles of potential sweeping at a scan rate of 100 mV/s in 3 M KOH. This activation treatment helped promote ion exchange reactions and enhance interfacial contacts between $K_2Ti_4O_9$ and Ni(OH)$_2$ and, hence, improved electrochemical stability. Figure 6a shows the CV curves of the $K_2Ti_4O_9$/Ti and $K_2Ti_4O_9$@Ni(OH)$_2$/Ti electrodes recorded at 50 mV/s in an aqueous solution of 3 M KOH. It can be seen that the voltammetric currents are about 2 orders of magnitude higher with $K_2Ti_4O_9$@Ni(OH)$_2$/Ti than with $K_2Ti_4O_9$/Ti. In addition, $K_2Ti_4O_9$@Ni(OH)$_2$/Ti exhibits a pair of voltammetric peaks at +0.34 V and +0.16 V, which are likely due to the redox chemistry of Ni(II) in the composite materials. This is distinctly different from that of $K_2Ti_4O_9$ where the primary contribution is from double-layer charging (Figure 2). The areal capacitance of $K_2Ti_4O_9$@Ni(OH)$_2$/Ti calculated from the CV curve at 50 mV/s is 340 mF/cm^2. In addition, the respective specific capacitance at 50 mV/s was calculated to be 11 F/g for $K_2Ti_4O_9$ and 319 F/g for $K_2Ti_4O_9$@Ni(OH)$_2$. Figure 6b shows the galvanostatic charging/discharging curves of $K_2Ti_4O_9$@Ni(OH)$_2$/Ti at different current densities. The areal capacitance was 276.3 mF/cm^2 at the discharge current density of 0.5 mA/cm^2, 173 mF/cm^2 at 1 mA/cm^2, and 72.5 mF/cm^2 at 5 mA/cm^2 (Figure S3).

The cycling performance of $K_2Ti_4O_9$@Ni(OH)$_2$/Ti at a current density of 1 mA/cm^2 is shown in Figure 6c. The $K_2Ti_4O_9$@Ni(OH)$_2$/Ti electrode possessed a high areal capacitance of 173 mF/cm^2 at the first charge/discharge cycle, which decreased only slightly to 161 mF/cm^2 after 800 cycles (93.0% retention) and remained virtually invariant thereafter (for instance, after 2000 cycles, the capacitance was 160 mF/cm^2). The shape of the last 10 charge–discharge curves (inset to Figure 6c) is almost unchanged, indicating good cyclability of the $K_2Ti_4O_9$@Ni(OH)$_2$/Ti electrode. Importantly, the $K_2Ti_4O_9$@Ni(OH)$_2$/Ti electrode shows apparently higher specific capacitance than many TiO_2-based electrodes reported previously, such as MnO_2/H-TiO_2 (19 mF/cm^2 at 50 mV/s in 0.5 M Na_2SO_4 solution),[9] V_2O_5/TiO_2 nanotube arrays (220 F/g in 0.1 M $HClO_4$),[24] TiN nanowire arrays (123 F/g at 10 mV/s in 1 M KOH),[23] and TiO_2/reduced graphene oxide (150 F/g at 0.4 A/g in Li half-cell),[28] which were summarized in Table S1. In addition, electrochemical impedance spectroscopy (EIS) measurements were also carried out to characterize the composite electrodes (Figure 6d). The equivalent series resistance (ESR) of $K_2Ti_4O_9$/Ti and $K_2Ti_4O_9$@Ni(OH)$_2$/Ti was both very low at 4.2 Ω and 5.6 Ω, respectively. This is probably due to the layered structures of the titanate backbones that facilitated charge transport along the axial direction.

For safety consideration and practical applications, all-solid-state supercapacitors are generally desired, as compared to their counterparts with liquid electrolytes, which require robust encapsulation to prevent leakage of the liquid electrolyte and other package components and hence are rather bulky. Thus, in the present study we also assembled two $K_2Ti_4O_9$@Ni(OH)$_2$/Ti electrodes to prepare a flexible solid-state supercapacitor with a KOH/PVA electrolyte. Figure 7a shows the CV curves of the $K_2Ti_4O_9$@Ni(OH)$_2$/Ti flexible solid-state supercapacitor at the potential scan rates of 5, 10, 20, 50, and 100 mV/s within the potential range of −0.4 to +0.4 V. The rectangular shapes of the CVs indicate excellent capacitive behaviors, even at the potential scan rate of 100 mV/s. The capacitance values

dx.doi.org/10.1021/am500421r | ACS Appl. Mater. Interfaces 2014, 6, 4578–4586

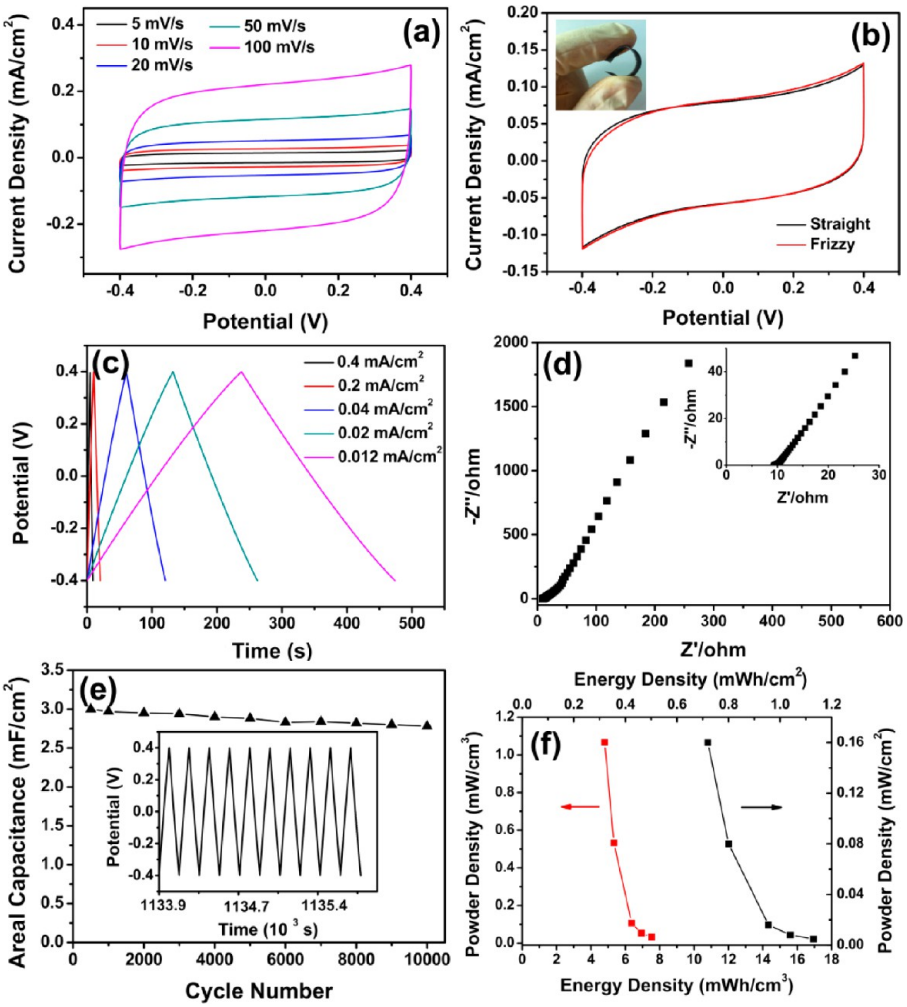

Figure 7. (a) CV curves of a flexible solid-state supercapacitor based on $K_2Ti_4O_9$@Ni(OH)$_2$/Ti. (b) Comparison of CV curves at 20 mV/s for a solid-state supercapacitor as straight and frizzy. Inset is the photograph of the $K_2Ti_4O_9$@Ni(OH)$_2$/Ti solid-state supercapacitor. (c) Galvanostatic charge/discharge curves of a flexible solid-state supercapacitor. (d) Nyquist plots of a $K_2Ti_4O_9$@Ni(OH)$_2$/Ti solid-state supercapacitor. (e) Cycling stability of a solid-state supercapacitor at the current density of 0.04 mA/cm^2. Inset: The last 10 charge−discharge curves. (f) Ragone plot of energy density (E) versus power density (P) for the $K_2Ti_4O_9$@Ni(OH)$_2$/Ti solid-state supercapacitor.

calculated from the CV curve at 5 mV/s and galvanostatic charge/discharge at 0.04 mA/cm^2 are 5.8 mF/cm^2 (Figure S4) and 3 mF/cm^2 (Figure S5), respectively. Furthermore, the solid state supercapacitor showed excellent mechanical integrity with no significant change of the electrochemical performance after mechanical stress of more than 200 intentional bends to a radius of about 1.5 cm, as manifested in CV measurements in the straight and frizzy shapes (Figure 7b).

In addition, rate capability is a key factor for practical applications of supercapacitors. For the $K_2Ti_4O_9$@Ni(OH)$_2$/Ti solid-state supercapacitors, the capacitance estimated from galvanostatic charge/discharge curves exhibited only a small decrease from 3.53 mF/cm^2 to 2.25 mF/cm^2 when the discharge current density was increased by 33 folds from 0.012 to 0.4 mA/cm^2. All charge/discharge curves of the $K_2Ti_4O_9$@Ni(OH)$_2$/Ti flexible solid-state supercapacitors at various current densities are triangular and symmetrical, indicating fast charging/discharging dynamics, and the ESR value was only 47.5 Ω (Figure 7d), though higher than that in a liquid electrolyte (e.g., 5.6 Ω in 3 M KOH, Figure 6d). Furthermore, the supercapacitors showed long-term stability. For instance, after 10 000 charge/discharge cycles at 0.04 mA/cm^2, the Coulombic efficiency was about 92.7% with only a small decrease from 3 to 2.78 mF/cm^2 (Figure 7e). To further evaluate the performance of the $K_2Ti_4O_9$@Ni(OH)$_2$/Ti electrode for all solid-state supercapacitors, the energy density (E) and power density (P) were calculated from the charge/discharge curves (Figure 7f). The $K_2Ti_4O_9$@Ni(OH)$_2$/Ti capacitor shows an energy density of 4.8 mWh/cm^3 (0.72 mWh/cm^2) at a power density of 1.1 mW/cm^3 (0.16 mW/cm^2) and still retains 7.5 mWh/cm^3 (1.13 mWh/cm^2) at a power density of 0.32 mW/cm^3 (0.048 mW/cm^2), which are higher than those of TiN nanowires (0.05 mWh/cm^3, PVA/KOH),[23] graphene-cellulose paper (0.015 mWh/cm^2, PVA/H_2SO_4),[29] and coaxial fiber (0.0098 mWh/cm^2 corresponding to a power density of 0.189 mW/cm^2, PVA/H_3PO_4),[30] which were summarized in Table S2.

This high rate capability of the $K_2Ti_4O_9$@Ni(OH)$_2$/Ti flexible solid-state supercapacitor might be accounted for by the following factors. First, the Ti mesh substrate exhibited high electrical conductivity and could effectively collect and transfer charges. Second, the layered structure of the $K_2Ti_4O_9$ nanowires provided effective paths for charge transport along the layer direction, without the use of polymer binders and

dx.doi.org/10.1021/am500421r | ACS Appl. Mater. Interfaces 2014, 6, 4578−4586

conductive additives in the electrodes. Third, Ni^{2+} ion-exchange reactions with the open layers of titanate led to the formation of intimate interfacial contacts between the $Ni(OH)_2$ nanosheets and the $K_2Ti_4O_9$ nanowires. Fourth, the growth of $Ni(OH)_2$ nanosheets on the surface of $K_2Ti_4O_9$ nanowires ($K_2Ti_4O_9$@$Ni(OH)_2$) produced a high specific surface area that facilitated fast and reversible redox reactions and hence improved specific capacitance.

CONCLUSIONS

In summary, a simple and effective route based on low temperature reactions and nickel ion-exchange reactions was developed for the preparation of $K_2Ti_4O_9$ nanowires coated with a shell of $Ni(OH)_2$ nanosheets that formed a highly porous network on the surface of a Ti mesh, i.e., $K_2Ti_4O_9$@$Ni(OH)_2$/Ti. Detailed electrochemical characterizations showed that the $K_2Ti_4O_9$@$Ni(OH)_2$/Ti electrode exhibited a high specific capacitance of 319 F/g at 50 mV/s in 3 M KOH and an areal capacitance of 340 mF/cm^2 with excellent cycling performance (93% retention after 2000 cycles), a few tens of times better than that of the unmodified $K_2Ti_4O_9$/Ti electrode. The $K_2Ti_4O_9$@$Ni(OH)_2$/Ti electrodes were also used to assemble a flexible solid-state supercapacitor with a PVA/KOH solid electrolyte, which showed outstanding electrochemical performance and excellent mechanical properties, with a high areal capacitance of 5.8 mF/cm^2 at 5 mV/s and remarkable cyclic stability (about 92.7% retention of capacitance after 10 000 charge−discharge cycles at 0.04 mA/cm^2). The results presented herein highlight the significance of deliberate interfacial engineering in the development of low-cost, large-scale, and practical supercapacitor electrodes and manipulation of the supercapacitor performance.

ASSOCIATED CONTENT

Supporting Information

Tabular comparison of specific capacitance with literature results, variation of areal capacitance with potential scan rate in solution and in solid-state supercapacitors, XRD patterns of $K_2Ti_4O_9$@$Ni(OH)_2$ powders from $K_2Ti_4O_9$@$Ni(OH)_2$/Ti. This material is available free of charge via the Internet at http://pubs.acs.org.

AUTHOR INFORMATION

Corresponding Authors

*E-mail: eszhouwj@scut.edu.cn.
*E-mail: shaowei@ucsc.edu.

Author Contributions

The manuscript was written through contributions of all authors. All authors have given approval to the final version of the manuscript.

Notes

The authors declare no competing financial interest.

ACKNOWLEDGMENTS

This work was supported by the Recruitment Program of Global Experts, the Ph.D. Start-up Funds of the Natural Science Foundation of Guangdong Province (S2013040016465), Zhujiang New Stars of Science & Technology, and the Fundamental Research Funds for Central Universities, China.

REFERENCES

(1) Stoller, M. D.; Ruoff, R. S. Best Practice Methods for Determining an Electrode Material's Performance for Ultracapacitors. *Energy Environ. Sci.* **2010**, *3*, 1294−1301.
(2) Simon, P.; Gogotsi, Y. Materials for Electrochemical Capacitors. *Nat. Mater.* **2008**, *7*, 845−854.
(3) Miller, J. R.; Outlaw, R. A.; Holloway, B. C. Graphene Double-Layer Capacitor with ac Line-Filtering Performance. *Science* **2010**, *329*, 1637−1639.
(4) Lu, X.; Zhai, T.; Zhang, X.; Shen, Y.; Yuan, L.; Hu, B.; Gong, L.; Chen, J.; Gao, Y.; Zhou, J.; Tong, Y.; Wang, Z. L. WO_3−x@Au@MnO_2 Core−Shell Nanowires on Carbon Fabric for High-performance Flexible Supercapacitors. *Adv. Mater.* **2012**, *24*, 938−944.
(5) Qu, Q.; Yang, S.; Feng, X. 2D Sandwich-like Sheets of Iron Oxide Grown on Graphene as High Energy Anode Material for Supercapacitors. *Adv. Mater.* **2011**, *23*, 5574−5580.
(6) Wu, Z.-S.; Ren, W.; Wen, L.; Gao, L.; Zhao, J.; Chen, Z.; Zhou, G.; Li, F.; Cheng, H.-M. Graphene Anchored With Co_3O_4 Nanoparticles as Anode of Lithium ion Batteries With Enhanced Reversible Capacity and Cyclic Performance. *ACS Nano* **2010**, *4*, 3187−3194.
(7) Dong, S.; Chen, X.; Gu, L.; Zhou, X.; Li, L.; Liu, Z.; Han, P.; Xu, H.; Yao, J.; Wang, H.; Zhang, X.; Shang, C.; Cui, G.; Chen, L. One Dimensional MnO_2/Titanium Nitride Nanotube Coaxial Arrays for High Performance Electrochemical Capacitive Energy Storage. *Energy Environ. Sci.* **2011**, *4*, 3502−3508.
(8) Wang, H.; Casalongue, H. S.; Liang, Y.; Dai, H. $Ni(OH)_2$ Nanoplates Grown on Graphene as Advanced Electrochemical Pseudocapacitor Materials. *J. Am. Chem. Soc.* **2010**, *132*, 7472−7477.
(9) Lu, X.; Wang, G.; Zhai, T.; Yu, M.; Gan, J.; Tong, Y.; Li, Y. Hydrogenated TiO_2 Nanotube Arrays for Supercapacitors. *Nano Lett.* **2012**, *12*, 1690−1696.
(10) Liu, J.; Jiang, J.; Cheng, C.; Li, H.; Zhang, J.; Gong, H.; Fan, H. J. Co_3O_4 Nanowire@MnO_2 ultrathin nanosheet core-shell arrays: A new class of high-performance pseudocapacitive Materials. *Adv. Mater.* **2011**, *23*, 2076−2081.
(11) Li, Q.; Wang, Z.-L.; Li, G.-R.; Guo, R.; Ding, L.-X.; Tong, Y.-X. Design and Synthesis of MnO_2/Mn/MnO_2 Sandwich-Structured Nanotube Arrays With High Supercapacitive Performance for Electrochemical Energy-storage. *Nano Lett.* **2012**, *12*, 3803−3807.
(12) Zhou, W.; Cao, X.; Zeng, Z.; Shi, W.; Zhu, Y.; Yan, Q.; Liu, H.; Wang, J.; Zhang, H. One-step Synthesis of Ni_3S_2 Nanorod@$Ni(OH)_2$ Nanosheet Core-Shell Nanostructures on Three-dimensional Graphene Network for High-Performance Supercapacitors. *Energy Environ. Sci.* **2013**, *6*, 2216−2221.
(13) Hu, C.-C.; Chang, K.-H.; Lin, M.-C.; Wu, Y.-T. Design and Tailoring of the Nanotubular Arrayed Architecture of Hydrous RuO_2 for Next Generation Supercapacitors. *Nano Lett.* **2006**, *6*, 2690−2695.
(14) Britvin, S. N.; Lotnyk, A.; Kienle, L.; Krivovichev, S. V.; Depmeier, W. Layered Hydrazinium Titanate: Advanced Reductive Adsorbent and Chemical Toolkit for Design of Titanium Dioxide Nanomaterials. *J. Am. Chem. Soc.* **2011**, *133*, 9516−9525.
(15) Xiong, Z.; Zhao, X. S. Nitrogen-Doped Titanate-Anatase Core−Shell Nanobelts with Exposed {101} Anatase Facets and Enhanced Visible Light Photocatalytic Activity. *J. Am. Chem. Soc.* **2012**, *134*, 5754−5757.
(16) Zhou, W.; Yin, Z.; Du, Y.; Huang, X.; Zeng, Z.; Fan, Z.; Liu, H.; Wang, J.; Zhang, H. Synthesis of Few-Layer MoS_2 Nanosheet-Coated TiO_2 Nanobelt Heterostructures for Enhanced Photocatalytic Activities. *Small* **2013**, *9*, 140−147.
(17) Yang, S.; Feng, X.; Müllen, K. Sandwich-Like, Graphene-Based Titania Nanosheets with High Surface Area for Fast Lithium Storage. *Adv. Mater.* **2011**, *23*, 3575−3579.
(18) Zhou, W.; Liu, H.; Boughton, R. I.; Du, G.; Lin, J.; Wang, J.; Liu, D. One-Dimensional Single-Crystalline Ti−O Based Nanostructures: Properties, Synthesis, Modifications and Applications. *J. Mater. Chem.* **2010**, *20*, 5993−6008.
(19) Guan, C.; Liu, J.; Cheng, C.; Li, H.; Li, X.; Zhou, W.; Zhang, H.; Fan, H. J. Hybrid Structure of Cobalt Monoxide Nanowire@Nickel

Hydroxidenitrate Nanoflake Aligned on Nickel Foam for High-Rate Supercapacitor. *Energy Environ. Sci.* **2011**, *4*, 4496−4999.
(20) Shirpour, M.; Cabana, J.; Doeff, M. New Materials Based on a Layered Sodium Titanate for Dual Electrochemical Na and Li Intercalation Systems. *Energy Environ. Sci.* **2013**, *6*, 2538−2547.
(21) Aziz, R. A.; Misnon, I. I.; Chong, K. F.; Yusoffa, M. M.; Josea, R. Layered sodium titanate nanostructures as a new electrode for high energy density supercapacitors. *Electrochim. Acta* **2013**, *113*, 141−148.
(22) Yang, F.; Yao, J.; Liu, F.; He, H.; Zhou, M.; Xiao, P.; Zhang, Y. Ni−Co oxides nanowire arrays grown on ordered TiO_2 nanotubes with high performance in supercapacitors. *J. Mater. Chem. A* **2013**, *1*, 594−601.
(23) Lu, X.; Wang, G.; Zhai, T.; Yu, M.; Xie, S.; Ling, Y.; Liang, C.; Tong, Y.; Li, Y. Stabilized TiN Nanowire Arrays for High-Performance and Flexible Supercapacitors. *Nano Lett.* **2012**, *12*, 5376−5381.
(24) Yang, Y.; Kim, D.; Yang, M.; Schmuki, P. Vertically Aligned Mixed V_2O_5−TiO_2 Nanotube Arrays for Supercapacitor Applications. *Chem. Commun.* **2011**, *47*, 7746−7748.
(25) Ambade, R. B.; Ambade, S. B.; Shrestha, N. K.; Nah, Y.-C.; Han, S.-H.; Lee, W.; Lee, S.-H. Polythiophene infiltrated TiO_2 nanotubes as high-performance supercapacitor electrodes. *Chem. Commun.* **2013**, *49*, 2308−2310.
(26) Zhou, W.; Wu, X.-J.; Cao, X.; Huang, X.; Tan, C.; Tian, J.; Liu, H.; Wang, J.; Zhang, H. Ni_3S_2 nanorods/Ni foam composite electrode with low overpotential for electrocatalytic oxygen evolution. *Energy Environ. Sci.* **2013**, *6*, 2921−2924.
(27) Buckley, A. N.; Woods, R. Electrochemical and XPS Studies of the Surface Oxidation of Synthetic Heazlewoodite (Ni_3S_2). *J. Appl. Electrochem.* **1991**, *21*, 575−582.
(28) Kim, H.; Cho, M.-Y.; Kim, M.-H.; Park, K.-Y.; Gwon, H.; Lee, Y.; Roh, K. C.; Kang, K. A Novel High-Energy Hybrid Supercapacitor with an Anatase TiO_2−Reduced Graphene Oxide Anode and an Activated Carbon Cathode. *Adv. Energy Mater.* **2013**, *3*, 1500−1506.
(29) Weng, Z.; Su, Y.; Wang, D.-W.; Li, F.; Du, J.; Cheng, H.-M. Graphene−Cellulose Paper Flexible Supercapacitors. *Adv. Energy Mater.* **2011**, *1*, 917−922.
(30) Le, V. T.; Kim, H.; Ghosh, A.; Kim, J.; Chang, J.; Vu, Q. A.; Pham, D. T.; Lee, J.-H.; Kim, S.-W.; Lee, Y. H. Coaxial Fiber Supercapacitor Using All-Carbon Material Electrodes. *ACS Nano* **2013**, *7*, 5940−5947.